Journal of Water Process Engineering 36 (2020) 101312

Contents lists available at ScienceDirect

Journal of Water Process Engineering

journal homepage: www.elsevier.com/locate/jwpe

Mechanistic models of electrocoagulation kinetics of pollutant removal in vinasse waste: Effect of voltage

Iqbal Syaichurrozi[a,b], Sarto Sarto[a,*], Wahyudi Budi Sediawan[a], Muslikhin Hidayat[a]

[a] Department of Chemical Engineering, Faculty of Engineering, Universitas Gadjah Mada, Jl. Grafika No. 2, Yogyakarta, 55281, Indonesia
[b] Department of Chemical Engineering, Faculty of Engineering, University of Sultan Ageng Tirtayasa, Jl. Jendral Soedirman Km 3, Cilegon, 42435, Indonesia

ARTICLE INFO

Keywords:
Electrocoagulation
Mechanistic models
Vinasse
Voltage
Waste

ABSTRACT

Vinasse is bioethanol liquid waste with high Chemical Oxygen Demand (COD) content, which is harmful to the environment. It therefore requires treatment and one of the potential methods to treat is electrocoagulation (EC). This process involved some mechanisms such as electrode dissolution, adsorption, entrapment, sedimentation and flotation. Furthermore, the working volume during the process, in reality, was not constant as it reduced. Hence, mechanistic models of EC were employed to have the detailed COD removal process. In this study, four mechanistic models were proposed and applied to simulate the COD removal process at voltage of 7.5 and 12.5 V. The results showed that Model 2 gave better prediction than the others due to its low Sum of Squares Error (SSE) which was 0.1189-0.2289 while the others showed SSE of 0.1884-0.5792. The model assumed that settled sludge was formed from the adsorption and entrapment of COD on the coagulants, while the floated sludge was formed from flotation of the settled sludge. Furthermore the model recorded higher kinetic constant values such as adsorption rate (k_a), entrapment rate (k_e) and flotation rate (k_f) at 12.5 V compared with those at 7.5 V. In conclusion, the proposed model successfully figured out the details of COD removal mechanisms during the EC of vinasse and the kinetic constant values increased with increase in voltage. It is expected that this model could be useful to predict the behavior of EC process with different conditions as well as to design EC system for industrial scales.

1. Introduction

Vinasse is a dark-brown final byproduct of bioethanol distillation with very low potential hydrogen (pH) level, within a range of 3.75–4.5 [1,2] and very high Chemical Oxygen Demand (COD) level, which is above 100 kg/m^3 [3,4]. This substance has a negative impact on the environment, especially photosynthesis in water plants due to decrease in the penetration rate of sun light. Also, the strong acidic nature of this substance results in remobilization of heavy metals in soil and its high COD content reduces the dissolved oxygen in water bodies, thereby affecting the respiration of biota, which leads to death [5]. The high ratio between bioethanol, which is the main product, and vinasse is 1 : 8–15 (v/v), this makes it constitute a serious problem for most industries [4]. Thus, there is need to treat it before being discharged into the water bodies.

There are various methods for treating vinasse such as anaerobic digestion [6,7], aerobic treatment [8], fungal treatment [9], Fenton [10], ozone [8,11] and electrocoagulation [12]. Chemical treatments, like the use of Fenton and ozone, are not efficient due to the high operating cost. Similarly, biological treatments, like anaerobic digestion, aerobic and fungal treatment, are not effective due to the high COD concentration of vinasse, which is toxic for biological activity. However, electrocoagulation (EC) has several advantages over the other methods, which include; (1) the use of simple equipments, (2) low operating cost, (3) short retention time, (4) easy to operate, (5) formation of less sludge compared with chemical coagulation [13–17]. Additionally, it does not need chemical additives, hence, highly applicable in green technologies [16,18,19].

Currently in Indonesia, the bioethanol industries are treating vinasse through anaerobic digestion (AD). A previous study [6] reported that AD is an effective method for treating vinasse with COD level of approximately 75 kg/m^3. One of the processes involved in this method is dilution, but it is not an efficient way of decreasing the COD level due to the high resultant waste volume. The EC, on the other hand, has the potential of additionally employing AD in treating vinasse with very high level of pollutants. Hence, a major concern of this study is to employ EC in reducing the COD of vinasse to approximately 75 kg/m^3.

The EC method is similar to chemical coagulation but the former

* Corresponding author.
E-mail address: sarto@ugm.ac.id (S. Sarto).

https://doi.org/10.1016/j.jwpe.2020.101312
Received 8 October 2019; Received in revised form 18 April 2020; Accepted 18 April 2020

Nomenclature

A_R	Base area of EC reactor (m^2)
A_e	Active surface area of electrode (m^2)
b	Rate constant of increase in x (m/s)
C_{COD}	Concentration of *COD* (kg/m^3)
C_{Fe}	Concentration of Fe^{z+} (kg/m^3)
F	Faraday's constant (96,500 C/mol)
I	Current (A)
J	Current density (A/m^2)
k_o	Reaction rate constant for oxidation (/s)
k_r	Reaction rate constant for reduction (/s)
k_a	Reaction rate constant for adsorption (m^3/(kg.s))
k_e	Reaction rate constant for entrapment (/s)
k_f	Reaction rate constant for flotation (/s)
k_s	Reaction rate constant for sedimentation (/s)
α	Fraction of settled sludge per total sludge (kg/kg)
α-1	Fraction of floated sludge per total sludge (kg/kg)
k_1	Reaction rate constant in first order kinetic (/s)
k_2	Reaction rate constant in second order kinetic (m^3/(kg.s))
m_{COD}	Mass of *COD* (kg)
	Mass of Fe^{z+} (kg)
$m_{floated\ sludge}$	Mass of *floated sludge* (kg)
$m_{settled\ sludge}$	Mass of *settled sludge* (kg)
M_w	Molar mass of Fe (0.056 kg/mol)
t	Retention time (s)
v	Volume of vinasse (m^3)
x	Difference between vinasse height level at t and at t_0 (m)
z	Number of electron transfer (2 or 3)
κ	Conductivity (S/m)
l_e	Length of electrode (m)
w_e	Width of electrode (m)
t_e	Thickness of electrode (m)
G	Conductance (S)
K	Cell constant (/m)
V	Voltage (V)
R	Resistance (Ohm)
d	Distance between electrodes (m)
ρ	Resistivity (Ohm m)
Q	Energy (J)
ΔT	Increase in temperature (K)
C_p	Caloric capacity of solution (J/K)
n_{H_2}	Hydrogen amount (mol)
H	Number of hydrogen molecules generated per electron (½)
q	Charge loading (C/kg COD)

utilizes an electrical current to produce coagulants, while the latter uses chemical agents such as $FeCl_2$, $FeCl_3$, $Fe_2(SO_4)_3$, $FeSO_4$, etc. [16,19]. In addition, EC needs metals as anode and cathode which are immersed in the vinasse. One of the metals commonly used as electrodes is iron (Fe). Due to the applied current during this process, anode (Fe) is oxidized to Fe^{z+} ion, a process known as electrode dissolution, while water is reduced to OH^- ion and H_2 gas at cathode [20]. Thus, the Fe^{z+} reacts with OH^- to form insoluble coagulant of $Fe(OH)_z$. The coagulant and H_2 gas formed are responsible for removing pollutants in the form of COD in the wastewater [16,21]. The coagulants have the capacity of adsorbing the pollutants and then entrap the other pollutants, while the H_2 gas allows the pollutants to float on the solution surface [16,18,21]. Based on these, EC utilizes three traditional treatments which are electrochemistry, coagulation and flotation [16].

The route of removing pollutants through the coordination between the coagulant and H_2 gas during EC process has not been clearly reported prior to this research. These are the four configuration steps for removing pollutants, as proposed in this study.

Configuration 1:

The coagulant ($Fe(OH)_z$) adsorbs COD to form aggregates and through agitation entrap the other COD to form bigger aggregates. These eventually go down as settled sludge. Also, the H_2 gas formed by water reduction coagulates and brings the other COD to the surface as floated sludge. This phenomenon is called as flotation.

Configuration 2:

In a similar to configuration 1, the aggregates formed through adsorption and entrapment of COD on coagulant go down as settled sludge. Since the attractive force among settled sludge is low, H_2 gas breaks parts of it, which are then brought to the surface as floated sludge.

Configuration 3:

This is in contrast to configuration 2. The aggregates formed through adsorption and entrapment of COD on coagulant go up as floated sludge, and due to its size, parts of it go down as settled sludge.

Configuration 4:

In this configuration, the aggregates formed through adsorption and entrapment of COD on coagulant are removed in a way in which parts of it go up as floated sludge, while the other parts settle go down.

It is assumed by many authors that the working volume is constant, but in reality, it decreases due to the reduction process of water. In addition, increase in temperature due to high current could increase the volume reduction process through evaporation. Hence, the decrease in volume could not be ignored.

Also, different authors have used empirical models such as the first order, second order, Langmuir, Elovich and fractional power models to predict pollutant removal by EC [22–24]. However, these models are not mathematically developed based on the mechanisms of the process. Thus, the need for the development of mechanistic models useful in describing the mechanisms in various configuration steps for removing pollutants. In the other water treatment, Fern á ndez et al. [25] developed the kinetic model of soil bioremediation process. However, the new mechanistic models were proposed in this study, which involved some complex mechanisms in EC which could be quantitatively figured.

Therefore, the aim of this study was to develop the mechanistic models based on different important configurations with the capacity of figuring out the detailed COD removal mechanisms during EC of vinasse at different voltage. The complex models involved the decrease in COD concentration, production of coagulant mass, production of floated and settled sludge mass and the reduction in working volume. Meanwhile, in empirical models, the production of floated and settled sludge mass was not considered and then the working volume was assumed constant. It is hoped that the proposed mechanistic models would describe the COD removal process during the EC of the other wastewaters, especially for those with high level of pollutants. Additionally, the comparison between the mechanistic and popular empirical models, specifically, first and second order kinetics, was presented in this study. Also, due to the variation of voltage, the applied current was different and this helped in predicting the correlation between the charge loading and COD removal efficiency.

Moreover, this study presented some important information which could increase the knowledge in EC process of vinasse. Hence, the novelty of this study could be summarized as follows:

- Investigation of COD removal in vinasse during EC at different voltage.
- Study of the decrease in working volume and production of floated and settled sludge mass.
- Development and application of the new mechanistic models which

explain the COD removal mechanisms.
- Study of the comparison between the mechanistic and empirical models.
- Prediction of the correlation between charge loading and COD removal efficiency in EC of vinasse.

2. Mechanism of electrocoagulation process

The configurations proposed were then explained in more detail in this section. There were four configuration types with different assumptions for each configuration.

Configuration 1

Mechanism of EC process based on configuration 1 is shown in Fig. 1. All the processes were assumed to be irreversible. Also, the working volume was not constant. Forced by electrical current, the anode (Fe) was dissolved to form Fe^{z+} ion, as shown in Eq. (1). Then at the cathode, water was reduced to OH^- ion and H_2 gas, as shown in Eq. (2) [21].

$$Fe \xrightarrow{k_o} Fe^{z+} + ze \quad (1)$$

$$zH_2O + ze \xrightarrow{k_r} \frac{z}{2}H_2 + zOH^- \quad (2)$$

Fe^{z+} ion later reacted with OH^- to form insoluble coagulants of Fe $(OH)_z$ as depicted in Eq. (3).

$$Fe^{z+} + zOH^- \xrightarrow{\text{hydrolysis}} Fe(OH)_z \quad (3)$$

The coagulants neutralized and adsorbed the pollutants (COD) to form aggregates which went down as settled sludge, as shown in Eq. (4).

$$\text{Coagulant} + \text{COD} \xrightarrow{k_a} \text{settled sludge} \quad (4)$$

Due to the spontaneous hydrolysis of Fe^{z+} to form the coagulants, the rate-determining step was generation of Fe^{z+} ion electrolytically [26]. Thus, Eq. (4) could be rewritten as:

$$Fe^{z+} + \text{COD} \xrightarrow{k_a} \text{settled sludge} \quad (5)$$

During the formation of the settled sludge, the aggregates dragged the other pollutants, a phenomenon known as entrapment, as shown in Eq. (6).

$$\text{COD} \xrightarrow{k_e} \text{settled sludge} \quad (6)$$

Furthermore, COD was removed by flotation in which H_2 gas pushed the pollutant to the surface as floated sludge, as shown in Eq. (7).

$$\text{COD} \xrightarrow{k_f} \text{floated sludge} \quad (7)$$

Therefore, the main processes in this configuration are shown by Eqs. (5)–(7).

Configuration 2

Mechanism of EC process based on configuration 2 is depicted in Fig. 2. Processes are expressed in Eqs. (5) and (6), also occur in configuration 2. However, Eq. (7) is modified to Eq. (8).

$$\text{settled sludge} \xrightarrow{k_f} \text{floated sludge} \quad (8)$$

Configuration 3

Mechanism of EC process based on configuration 3 is depicted in Fig. 3. Processes expressed in Eqs. (5)–(7) are modified to Eqs. (9)–(11) respectively.

$$Fe^{z+} + \text{COD} \xrightarrow{k_a} \text{floated sludge} \quad (9)$$

$$\text{COD} \xrightarrow{k_e} \text{floated sludge} \quad (10)$$

$$\text{floated sludge} \xrightarrow{k_s} \text{settled sludge} \quad (11)$$

Configuration 4

Mechanism of EC process based on configuration 4 is depicted in Fig. 4. Three main processes expressed in Eqs. (5)–(7) are modified to become two main processes expressed by Eqs. (12) and (13).

$$Fe^{z+} + \text{COD} \xrightarrow{k_a} \text{floated sludge} + \text{settled sludge} \quad (12)$$

$$\text{COD} \xrightarrow{k_e} \text{floated sludge} + \text{settled sludge} \quad (13)$$

3. Modeling

Based on the configurations described in Section 2, the mathematical descriptions of the process were presented in this section. The setting up of the mathematical equations was basically the applications of material balances.

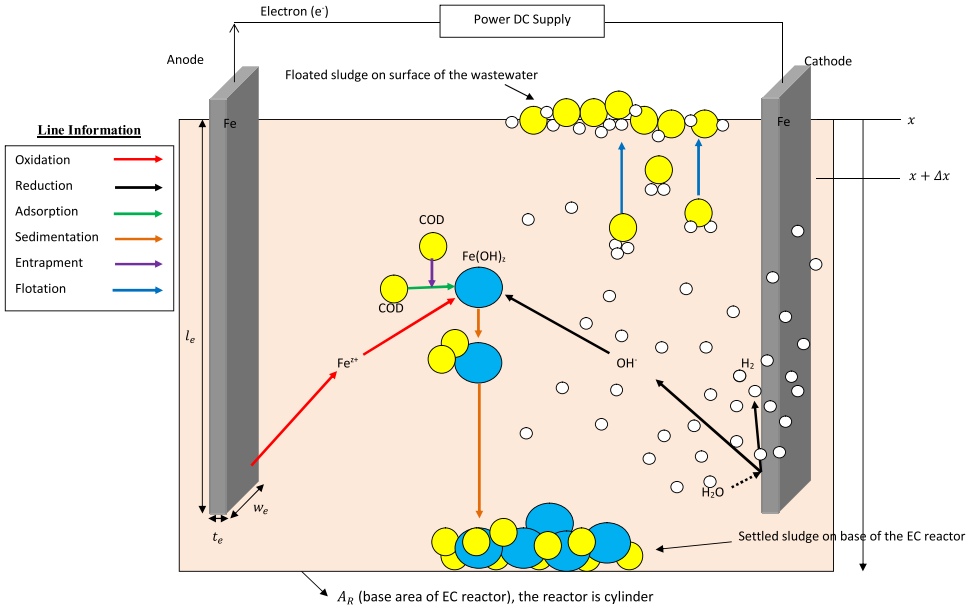

Fig. 1. Mechanism of COD removal during EC of vinasse based on configuration 1.

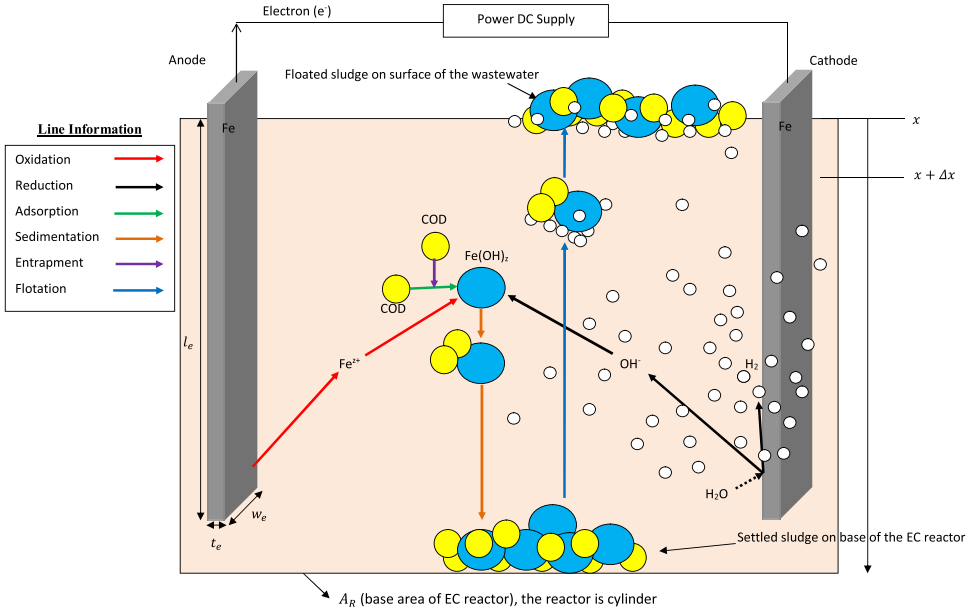

Fig. 2. Mechanism of COD removal during EC of vinasse based on configuration 2.

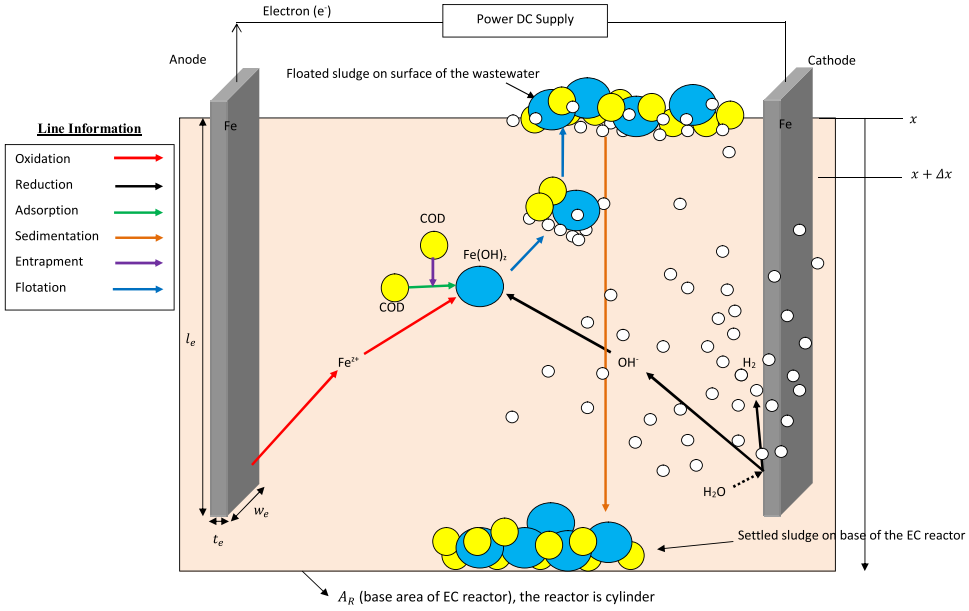

Fig. 3. Mechanism of COD removal during EC of vinasse based on configuration 3.

3.1. Model 1 (based on Configuration 1)

3.1.1. Electrode consumption

In EC process, electrode (anode) was oxidized to Fe^{z+} ion. The rate of the electrode consumption could be predicted through Faraday's law, as shown in Eq. (14) [26,27].

$$\frac{dm_{anode}}{dt} = -\frac{IM_w}{zF} \tag{14}$$

During the process, volume of vinasse decreased due to the reduction and evaporation processes. Since the base surface of EC reactor was constant, the vinasse surface level was observed to change during process. Hence, based on Fig. 1, the value of x increased during the EC process. As a consequent, the active surface of electrode decreased. Since $I = JA_e$ and $A_e = 2(l_e - x)w_e + 2(l_e - x)t_e + w_e t_e$, Eq. (14) is modified to Eq. (15).

$$\frac{dm_{anode}}{dt} = -\frac{JM_w(2(l_e - x)w_e + 2(l_e - x)t_e + w_e t_e)}{zF} \tag{15}$$

The rate of increase in x value (or decrease in surface level of working volume) could be expressed with a simple Eq. (16a).

$$\frac{dx}{dt} = b \tag{16a}$$

Integration of Eq. (16a) produces Eq. (16b):

$$\int_0^x dx = b\int_0^t dt$$
$$x = bt \tag{16b}$$

The value of b was obtained based on the observation of the surface levels at various times. It was discussed in Section 5.2.

Therefore, substitution of Eq. (16b) to Eq. (15) produces Eq. (17)

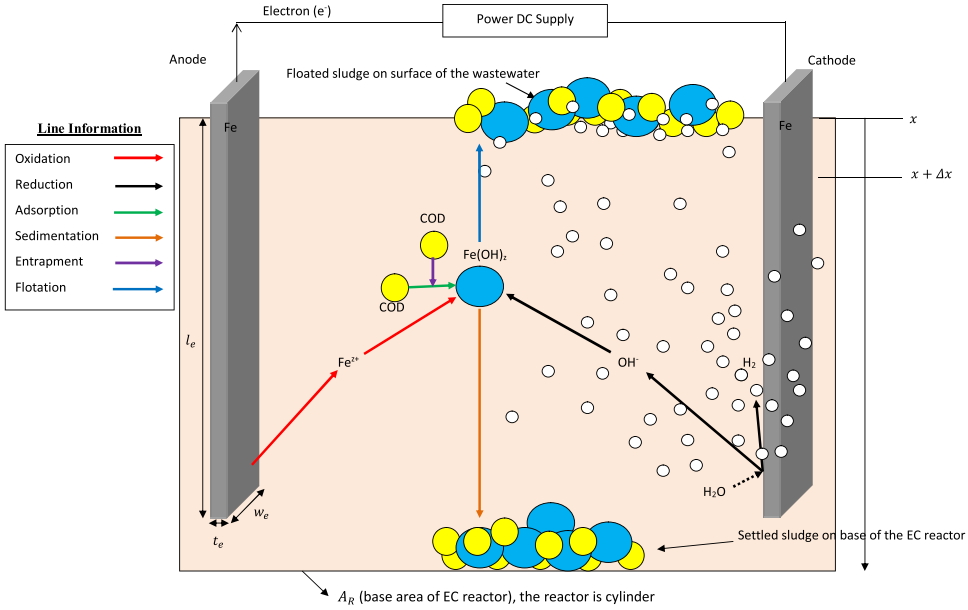

Fig. 4. Mechanism of COD removal during EC of vinasse based on configuration 4.

$$\frac{dm_{anode}}{dt} = -\frac{JM_w(2(l_e - bt)w_e + 2(l_e - bt)t_e + w_e t_e)}{zF} \tag{17}$$

3.1.2. Net rate of Fe^{z+} mass

Fe^{z+} mass was produced through the oxidation of anode, while it was consumed through the adsorption process. Net rate of Fe^{z+} mass is the difference between the production and consumption rates of Fe^{z+} mass. Thus, net rate of Fe^{z+} mass during EC is shown in Eq. (18).

$$\frac{dm_{Fe}}{dt} = \frac{JM_w(2(l_e - bt)w_e + 2(l_e - bt)t_e + w_e t_e)}{zF} - k_a C_{Fe} C_{COD} v \tag{18}$$

Since $m_{Fe} = C_{Fe}v$, $v = v_0 - A_R x$ and $x = bt$, Eq. (18) is modified to Eq. (19).

$$\begin{aligned}
\frac{d(C_{Fe}v)}{dt} &= \frac{JM_w(2(l_e - bt)w_e + 2(l_e - bt)t_e + w_e t_e)}{zF} - k_a C_{Fe} C_{COD}(v_0 - A_R bt)\\
C_{Fe}\frac{dv}{dt} + v\frac{dC_{Fe}}{dt} &= \frac{JM_w(2(l_e - bt)w_e + 2(l_e - bt)t_e + w_e t_e)}{zF}\\
&\quad - k_a C_{Fe} C_{COD}(v_0 - A_R bt)\\
C_{Fe}\frac{d(v_0 - A_R bt)}{dt} + (v_0 - A_R bt)\frac{dC_{Fe}}{dt} &= \frac{JM_w(2(l_e - bt)w_e + 2(l_e - bt)t_e + w_e t_e)}{zF}\\
&\quad - k_a C_{Fe} C_{COD}(v_0 - A_R bt)\\
-C_{Fe}A_R b + (v_0 - A_R bt)\frac{dC_{Fe}}{dt} &= \frac{JM_w(2(l_e - bt)w_e + 2(l_e - bt)t_e + w_e t_e)}{zF}\\
&\quad - k_a C_{Fe} C_{COD}(v_0 - A_R bt)\\
\frac{dC_{Fe}}{dt} &= \frac{\frac{JM_w(2(l_e - bt)w_e + 2(l_e - bt)t_e + w_e t_e)}{zF} - k_a C_{Fe} C_{COD}(v_0 - A_R bt) + C_{Fe}A_R b}{(v_0 - A_R bt)}
\end{aligned} \tag{19}$$

3.1.3. Net rate of COD mass

Decrease in COD mass was caused by the adsorption, entrapment and flotation, as shown in Eq. (20).

$$\begin{aligned}
\frac{dm_{COD}}{dt} &= -k_a C_{Fe} C_{COD} v - k_e C_{COD} v - k_f C_{COD} v\\
\frac{d(C_{COD}v)}{dt} &= -k_a C_{Fe} C_{COD} v - k_e C_{COD} v - k_f C_{COD} v
\end{aligned} \tag{20}$$

Since $m_{COD} = C_{COD}v$, $v = v_0 - A_R x$ and $x = bt$, Eq. (20) is modified to Eq. (21).

$$\begin{aligned}
C_{COD}\frac{dv}{dt} + v\frac{dC_{COD}}{dt} &= C_{COD}v(-k_a C_{Fe} - k_e - k_f)\\
(-C_{COD}A_R b) + (v_0 - A_R bt)\frac{dC_{COD}}{dt}&\\
= C_{COD}(v_0 - A_R bt)(-k_a C_{Fe} - k_e - k_f)&\\
\frac{dC_{COD}}{dt} &= \frac{C_{COD}(v_0 - A_R bt)(-k_a C_{Fe} - k_e - k_f) + (C_{COD}A_R b)}{(v_0 - A_R bt)}
\end{aligned} \tag{21}$$

3.1.4. Net rate of settled sludge mass

Increase in settled sludge mass was caused by adsorption and entrapment, as shown in Eq. (22).

$$\begin{aligned}
\frac{dm_{settled\ sludge}}{dt} &= k_a C_{Fe} C_{COD} v + k_e C_{COD} v\\
\frac{dm_{settled\ sludge}}{dt} &= C_{COD} v(k_a C_{Fe} + k_e)
\end{aligned} \tag{22}$$

Since $v = v_0 - A_R x$ and $x = bt$, Eq. (22) is modified to Eq. (23).

$$\frac{dm_{settled\ sludge}}{dt} = C_{COD}(v_0 - A_R bt)(k_a C_{Fe} + k_e) \tag{23}$$

3.1.5. Net rate of floated sludge mass

Increase in floated sludge mass was caused by flotation, as shown in Eq. (24).

$$\frac{dm_{floated\ sludge}}{dt} = k_f C_{COD} v \tag{24}$$

Since $v = v_0 - A_R x$ and $x = bt$, Eq. (24) is modified to Eq. (25).

$$\frac{dm_{floated\ sludge}}{dt} = k_f C_{COD}(v_0 - A_R bt) \tag{25}$$

Table 1 shows the mathematical equations for Model 1 in detail.

3.2. Model 2 (based on Configuration 2)

Model 2 was built based on configuration 2. Hence, by modifying the mathematical equations in Model 1, the ones in Model 2 could be obtained and presented as in Table 2.

Table 1
Mathematical equations for Model 1 in EC of vinasse waste.

Rate	Equation
$\frac{dC_{Fe}}{dt}$	$\frac{JM_w(2(l_e-bt)w_e+2(l_e-bt)t_e+w_et_e)}{zF}-k_aC_{Fe}C_{COD}(v_0-A_Rbt)+C_{Fe}A_Rb}{(v_0-A_Rbt)}$
$\frac{dC_{COD}}{dt}$	$\frac{C_{COD}(v_0-A_Rbt)(-k_aC_{Fe}-k_e-k_f)+(C_{COD}A_Rb)}{(v_0-A_Rbt)}$
$\frac{dm_{settled\ sludge}}{dt}$	$C_{COD}(v_0-A_Rbt)(k_aC_{Fe}+k_e)$
$\frac{dm_{floated\ sludge}}{dt}$	$k_fC_{COD}(v_0-A_Rbt)$

Table 2
Mathematical equations for Model 2 in EC of vinasse waste.

Rate	Equation
$\frac{dC_{Fe}}{dt}$	$\frac{JM_w(2(l_e-bt)w_e+2(l_e-bt)t_e+w_et_e)}{zF}-k_aC_{Fe}C_{COD}(v_0-A_Rbt)+C_{Fe}A_Rb}{(v_0-A_Rbt)}$
$\frac{dC_{COD}}{dt}$	$\frac{C_{COD}(v_0-A_Rbt)(-k_aC_{Fe}-k_e)+(C_{COD}A_Rb)}{(v_0-A_Rbt)}$
$\frac{dm_{settled\ sludge}}{dt}$	$C_{COD}(v_0-A_Rbt)(k_aC_{Fe}+k_e)-k_fm_{settled\ sludge}$
$\frac{dm_{floated\ sludge}}{dt}$	$k_fm_{settled\ sludge}$

3.3. Model 3 (based on Configuration 3)

Model 3 was built based on configuration 3. Hence, by modifying the mathematical equations in Model 1, the ones in Model 3 could be obtained and presented in Table 3.

3.4. Model 4 (based on Configuration 4)

Model 4 was built based on configuration 4. Hence, by modifying the mathematical equations in Model 1, the ones in Model 4 could be obtained and presented in Table 4.

Table 3
Mathematical equations for Model 3 in EC of vinasse waste.

Rate	Equation
$\frac{dC_{Fe}}{dt}$	$\frac{JM_w(2(l_e-bt)w_e+2(l_e-bt)t_e+w_et_e)}{zF}-k_aC_{Fe}C_{COD}(v_0-A_Rbt)+C_{Fe}A_Rb}{(v_0-A_Rbt)}$
$\frac{dC_{COD}}{dt}$	$\frac{C_{COD}(v_0-A_Rbt)(-k_aC_{Fe}-k_e)+(C_{COD}A_Rb)}{(v_0-A_Rbt)}$
$\frac{dm_{settled\ sludge}}{dt}$	$k_sm_{floated\ sludge}$
$\frac{dm_{floated\ sludge}}{dt}$	$C_{COD}(v_0-A_Rbt)(k_aC_{Fe}+k_e)-k_sm_{floated\ sludge}$

Table 4
Mathematical equations for Model 4 in EC of vinasse waste.

Rate	Equation
$\frac{dC_{Fe}}{dt}$	$\frac{JM_w(2(l_e-bt)w_e+2(l_e-bt)t_e+w_et_e)}{zF}-k_aC_{Fe}C_{COD}(v_0-A_Rbt)+C_{Fe}A_Rb}{(v_0-A_Rbt)}$
$\frac{dC_{COD}}{dt}$	$\frac{C_{COD}(v_0-A_Rbt)(-k_aC_{Fe}-k_e)+(C_{COD}A_Rb)}{(v_0-A_Rbt)}$
$\frac{dm_{settled\ sludge}}{dt}$	$\alpha C_{COD}(v_0-A_Rbt)(k_aC_{Fe}+k_e)$
$\frac{dm_{floated\ sludge}}{dt}$	$(\alpha-1)C_{COD}(v_0-A_Rbt)(k_aC_{Fe}+k_e)$

3.5. Empirical models

As comparison with the proposed mechanistic models, some popular empirical models were also tried to quantitatively describe the measured data of COD concentration. The empirical models assume that the working volume is constant. Kinetic of decrease in COD concentration during EC batch process was simulated through the first and second order kinetic models, which are expressed in Eqs. (26) and (27) respectively [24,28,29].

First order kinetic

$$-\frac{dC_{COD}}{dt}=k_1C_{COD}$$
$$\ln C_{COD(t)}=\ln C_{COD(0)}-k_1t$$
$$C_{COD(t)}=\exp(\ln C_{COD(0)}-k_1t) \quad (26)$$

Second order kinetic

$$-\frac{dC_{COD}}{dt}=k_2C_{COD}^2$$
$$\frac{1}{C_{COD(t)}}=\frac{1}{C_{COD(0)}}+k_2t$$
$$C_{COD(t)}=\frac{C_{COD(0)}}{1+C_{COD(0)}k_2t} \quad (27)$$

4. Materials and methods

4.1. Vinasse

The raw form of vinasse was collected from a bioethanol industry in Indonesia. It was the same as the raw vinasse used by a previous study [12]. It had a pH value of 4.35 (acidic), contained COD of 100.16 kg/m^3 and total dissolved Fe of 0.039 kg/m^3.

4.2. Experimental set-up

This study used the same experimental set-up as a previous study [12]. The electrocoagulation reactor was made with 1 L glass beaker cylindrical in shape. It had a diameter of 0.11 m and height of 0.155 m with a working volume of 1000 mL (1×10^{-3} m^3). The length, width and thickness of electrodes used were 0.2, 0.03 and 0.003 m respectively. However, the active dimension of both the anode and cathode was length, width and thickness of 0.095, 0.03 and 0.003 m respectively, with active surface area (A_{e0}) of 0.00636 m^2. Also, the distance (d) between the electrodes was kept constant at 0.055 m [30]. The current was supplied through a Power DC supply (Long Wei, Series of LW-K3010D, 0–30 V, 0–10 A) and agitation speed was kept constant at 200 rpm.

4.3. Experimental design and procedures

Before used, the electrodes were soaked in HCl 5%v/v solution for 15 min and rinsed using aquadest and then weighted [12,31]. The initial pH of vinasse was adjusted 6.0 through the addition of NaOH (technical grade). The voltage was set at 7.5 and 12.5 V. The EC process was conducted in batch mode for 60 min (3600 s). In addition, replication of the experiment was not conducted. During process, the current was recorded every 10 min (600 s). The floated sludge on surface of vinasse was carefully and precisely taken using a plastic spoon. This was then dried at temperature range of 105–110 °C after which it was weighted. The temperature of vinasse was then measured using a mercury thermometer (with 0–100 °C range) while its pH was measured using a digital pH meter (model ATC 2011). Furthermore, 10 mL of the sample solution was placed in a reaction tube and allowed to settle down for 24 h [12]. The sampling of 10 mL every 600 s during EC process was considered to have no effect on the COD removal

mechanisms and volume reduction. In other words, the decrease in volume was assumed due to evaporation and reduction processes of water.

4.4. Analysis

4.4.1. The COD and total dissolved Fe concentration analysis

Upon settling, 5 mL of the supernatants were taken and diluted to 50 mL with aquadest (dilution factor of 10) for the COD and total dissolved Fe analysis. The COD analysis was conducted through open reflux and titration method of SNI 06-6989.15-2004, a method with capacity of measuring COD values in the range of 0.050 – 0.9 kg/m^3. Hence, there was need to dilute it again until the total dilution factor of 250. The chemicals used included potassium dichromate ($K_2Cr_2O_7$) 0.25 N, sulfuric acid reagent, ferrous ammonium sulfate (FAS) 0.1 N and ferroin indicator. The sulfuric acid reagent was prepared by dissolving 10.12 g Ag_2SO_4 in 1000 mL concentrated H_2SO_4. The FAS 0.1 N was prepared by dissolving 39.2 g $Fe(NH_4)_2(SO_4)_2.6H_2O$ in aquadest, after which 20 mL concentrated H_2SO_4 was added to the solution and allowed to cool at room temperature. Then, aquadest was added till the total volume was 1000 mL. The procedure of COD analysis was as follows: (1) 10 mL of the sample was put into a 250-mL Erlenmeyer flask, (2) 0.2 g $HgSO_4$, 5 mL $K_2Cr_2O_7$ 0.25 N, and 15 mL sulfuric acid reagent were added to it, (3) the Erlenmeyer flask was connected to a condenser after which it was heated on hot plate for 2 h, (4) the sample was allowed to cool at room temperature and then the inside of the condenser was washed using approximately 50 mL aquadest, (5) two to three drops of ferroin indicator were added to the sample, (6) the sample was titrated using FAS 0.1 N until the color changes to reddish brown and the volume of FAS used was recorded. Step 1 until 6 were also conducted for aquadest as the blank sample and the COD concentration was calculated using Eq. (28a). In addition, The FAS has to be standardized daily against $K_2Cr_2O_7$ 0.25 N. The FAS standardization procedure was as follows: (1) 5 mL $K_2Cr_2O_7$ 0.25 N was put into a 250-mL Erlenmeyer flask, (2) it was diluted to about 50 mL with aquadest, (3) 15 mL concentrated H_2SO_4 was added, (4) two to three drops of ferroin indicator were added, (5) it was titrated using FAS 0.1 N until the color changes to reddish brown and the volume of FAS used was recorded. The normality of FAS was calculated by using Eq. (28b).

$$COD = \frac{(V_{FAS\ for\ blank\ titration} - V_{FAS\ sample\ titration}).(N_{FAS}).\ 8000.\ total\ dilution\ factor}{V_{sample}} \quad (28a)$$

$$Normality\ of\ FAS = \frac{V_{\text{potassium dichromate}}.\ N_{\text{potassium dichromate}}}{V_{FAS}} \quad (28b)$$

The total dissolved Fe in the solution was measured through the analysis service in Badan Tenaga Nuklir Nasional (BATAN) using Atomic Absorption Spectroscopy (AAS). For preparation before AAS analysis, the sample was filtered using the Whatman grade 42 filter paper [32]. The total dissolved Fe data from BATAN was multiplied with dilution factor of 10. The measured total dissolved Fe was assumed that it represented the amount of total Fe^{z+} ions in the solution. The appropriate z value was discussed in Section 5.2.

4.4.2. The weight loss in anode and mass measurement of floated sludge

Upon completing the EC process, anode, the sacrificial electrode, was rinsed using distilled water and then dried within a temperature range of 105–110 °C, after which it was weighted. Similar to the explanation provided in Section 4.3, the floated sludge was carefully and precisely taken using a plastic spoon from the surface of vinasse. This was dried at a temperature range of 105–110 °C and weighted.

4.4.3. Mass estimation of settled sludge

The settled sludge mass was estimated using material balance as shown in Eq. (29a) and the Fe in total sludge (sum of floated and settled sludge) was estimated through Eq. (29b) while the Fe electrolytically produced was estimated with Eq. (29c). In the vinasse, the ratio of COD to total solid (TS) is close to one [4,33]. Since the TS is equal to sum of total dissolved solid (TDS) and total suspended solid (TSS), in other

Table 5
Summary of experimental data during EC of vinasse waste at voltage of 7.5 and 12.5 V.

7.5 V t (s)	I (A)	T (K)	pH	x ($\times10^{-2}$ m)	Volume ($\times10^{-6}$ m^3)	Floated sludge ($\times10^{-3}$ kg)	COD kg/m^3	COD $\times10^{-3}$ kg	COD Mass removal (%)	Total dissolved Fe kg/m^3	Total dissolved Fe $\times10^{-3}$ kg	Anode weight loss ($\times10^{-3}$ kg)	J (A/m^2)	R (Ohm)	ρ (Ohm m)	κ (S/m)
0	2.15	302.65	6.0	0.00	1000.00	0.00	100.16	100.16	0.00	0.039	0.039	0	338.05	3.49	0.403	2.479
600	2.16	304.15	6.1	0.20	981.00	0.28	97.36	95.51	4.64	Na	Na	Na	346.82	3.47	0.393	2.543
1200	2.20	306.65	6.1	0.45	957.26	1.42	92.87	88.91	11.24	0.398	0.381	Na	362.86	3.41	0.376	2.661
1800	2.22	307.35	6.4	0.65	938.26	2.78	92.65	86.93	13.21	Na	Na	Na	374.30	3.38	0.364	2.745
2400	2.18	308.65	6.6	0.85	919.26	4.05	92.65	85.17	14.97	0.923	0.849	Na	375.93	3.44	0.363	2.757
3000	2.10	309.65	6.8	1.05	900.27	5.30	91.08	81.99	18.14	Na	Na	Na	370.57	3.57	0.368	2.717
3600	2.05	310.15	7.2	1.25	881.27	6.90	91.08	80.26	19.87	0.886	0.781	−2.241	370.37	3.66	0.368	2.716
12.5 V t (s)	I (A)	T (K)	pH	x ($\times10^{-2}$ m)	Volume ($\times10^{-6}$ m^3)	Floated sludge ($\times10^{-3}$ kg)	COD kg/m^3	COD $\times10^{-3}$ kg	COD Mass removal (%)	Total dissolved Fe kg/m^3	Total dissolved Fe $\times10^{-3}$ kg	Anode weight loss ($\times10^{-3}$ kg)	J (A/m^2)	R (Ohm)	ρ (Ohm m)	κ (S/m)
0	3.76	302.15	6.0	0.00	1000.00	0.00	100.16	100.16	0.00	0.039	0.039	0	591.19	3.32	0.384	2.601
600	4.17	308.65	6.3	0.90	914.51	1.54	95.79	87.60	12.54	Na	Na	Na	723.20	3.00	0.314	3.182
1200	4.25	314.65	6.8	1.60	848.02	5.32	92.65	78.57	21.56	0.560	0.475	Na	801.28	2.94	0.284	3.526
1800	4.26	319.85	7.5	2.15	795.78	9.47	91.08	72.48	27.64	Na	Na	Na	862.17	2.93	0.264	3.794
2400	4.08	324.35	7.7	2.75	738.79	14.44	87.94	64.97	35.14	0.529	0.391	Na	897.69	3.06	0.253	3.950
3000	3.88	328.15	7.7	3.75	643.81	19.35	84.80	54.59	45.50	Na	Na	Na	998.71	3.22	0.228	4.394
3600	3.53	330.65	7.3	4.40	582.07	26.78	83.17	48.41	51.67	0.490	0.285	−4.328	1021.41	3.54	0.223	4.494

Remarks = I, current; T, temperature; x, decrease in surface level of vinasse; COD, chemical oxygen demand; J, current density; R, resistance; ρ, resistivity; κ, conductivity; Na, not analyzed.

words, the COD value was almost same with sum of total suspended solid (TSS) and total dissolved solid (TDS). It means that the vinasse dominantly contained organic pollutants. The other pollutants, which were inorganic materials, not measured as COD, were in little amount [5], hence this study assumed that the settled and floated sludge were formed mainly by the COD removal in vinasse and Fe in total sludge.

$$\textit{Settled sludge mass} = \textit{removed COD mass} - \textit{floated sludge mass} + \textit{Fe mass in total sludge} \quad (29a)$$

$$\textit{Fe mass in total sludge} = \textit{initial Fe mass} + \textit{Fe mass produced electrolytically} - \textit{remaining Fe mass in solution} \quad (29b)$$

$$\frac{dm_{Fe\ produced\ electrolytically}}{dt} = \frac{JM_w(2(l_e - bt)w_e + 2(l_e - bt)t_e + w_e t_e)}{zF} \quad (29c)$$

4.4.4. The conductivity and resistivity estimation

The solution conductivity could be estimated using Eq. (30) [34]. Since $G = \frac{1}{R}$, $R = \frac{V}{I}$ and $K = \frac{d}{A_e}$, Eq. (30) is modified to Eq. (31). Meanwhile, resistivity was estimated using Eq. (32)

$$\kappa = G.K \quad (30)$$

$$\kappa = \frac{1}{R}.\frac{d}{A_e} \quad (31)$$

$$\rho = \frac{1}{\kappa} \quad (32)$$

4.5. Kinetic analysis

The measured data during EC process were COD, total dissolved Fe in solution, floated sludge and settled sludge at various times. The adjustable parameters in Model 1 and 2 were k_a, k_e, k_f, the ones in Model 3 were k_a, k_e, k_s while the ones in Model 4 were k_a, k_e, α. The values of these parameters were obtained through the minimization of Sum of Squares Error (SSE). The simultaneous ordinary differential equations were solved through ode15s and minimization of SSE was through fminsearch with help of MATLAB software. The SSE was presented in Eq. (33).

$$\text{SSE} = \sum_{i=1}^{n}\left(\frac{measured\ data_i - predicted\ data_i}{measured\ data_i}\right)^2 \quad (33)$$

Furthermore, curve fitting between the experimental data and calculated results was also conducted.

5. Results and discussions

The EC was successfully conducted at voltage of 7.5 and 12.5 V. This voltage difference had effects on the measured data such as current density, pH, temperature, COD, total dissolved Fe and floated sludge during EC, as presented in Table 5. Also, the four proposed mechanistic models were applied to fit the measured data and the best one, having the lowest SSE value, was compared with the empirical models, mainly the first and second order kinetic models in fitting of the COD concentration during EC of vinasse. Furthermore, the effect of charge loading on the COD removal efficiency was estimated. The detailed results and discussions were presented in the Section of 5.1–5.8.

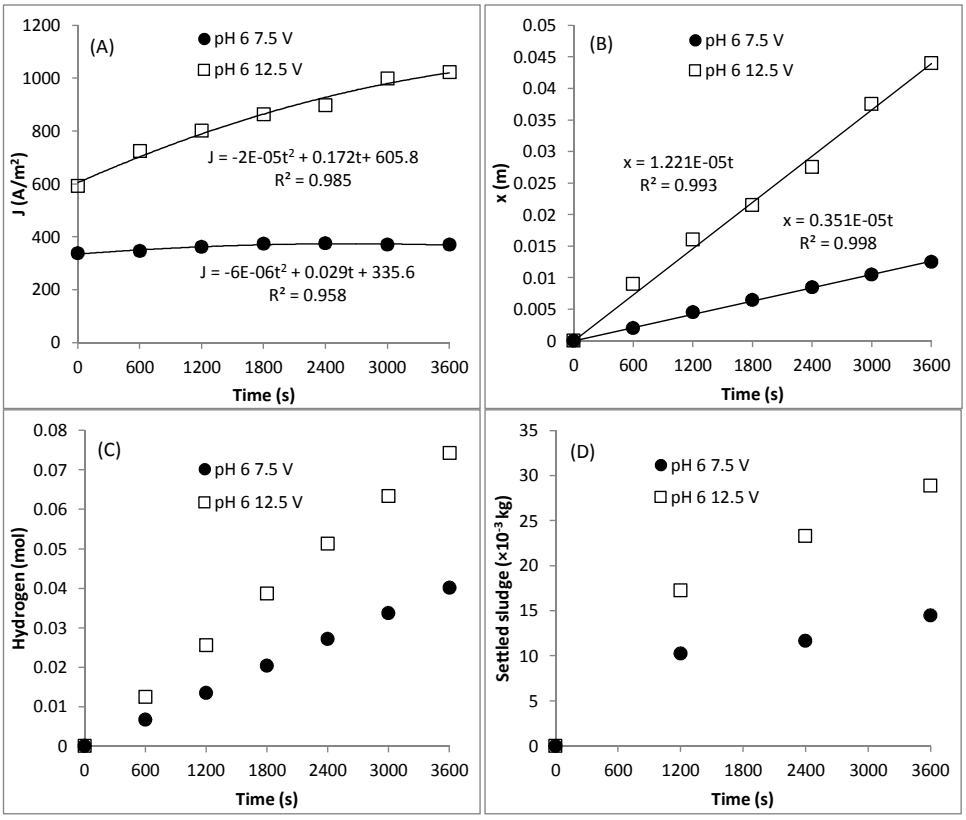

Fig. 5. (A) current density profile, (B) decrease in vinasse surface level in EC reactor, (C) prediction of hydrogen gas production, (D) settled sludge mass profile during EC of vinasse waste.

5.1. Current density profile

The change in current (I) during EC process of vinasse at voltage of 7.5 V and 12.5 V was recorded and shown in Table 5. Also, the decrease in vinasse surface level (x) in EC reactor was measured and presented in Table 5. The active surface of electrodes decreased due to the increase in x, which was calculated per real time using the formula, $A_e = 2(l_e - x)w_e + 2(l_e - x)t_e + w_e t_e$. Additionally, the current density (J) was calculated using the formula, I/A_e, as shown in Table 5, and the change in J as a function of time (t) is presented in Fig. 5(A).

Based on the results, the current density increased drastically at voltage of 12.5 V. Thus, the higher the voltage, the higher the current was supplied to solution, thereby causing the production of Fe^{z+} ion in large amount. The presence of these ions subsequently increased the solution conductivity thereby allowing the current to flow with ease. However, the current density increased slowly at 7.5 V leading to the generation of Fe^{z+} ion in low quantities. Also considering Table 5, the solution conductivity at 12.5 V was higher than that at 7.5 V, but the solution resistivity at 12.5 V was lower than that at 7.5 V.

5.2. Determining the z value

During EC, the anode (Fe) was oxidized to be Fe^{z+} ion. Based on the works of some authors [35–38], z was assigned 2, hence, Fe^{2+} (ferrous) was produced from oxidation of Fe. Other authors [39,40], however, assigned 3 to it, resulting in Fe^{3+} (ferric).

To find the suitable z value, the anode weight was measured before and after the process. The weight after the process was also predicted using Eq. (17) with z = 2 and 3. The value of b was obtained by making a plot between x (m) and t (s) as shown in Fig. 5(B) where it at 7.5 and 12.5 V was 0.351×10^{-5} and 1.221×10^{-5} m/s respectively. Then, the anode weights after the process were 2.241×10^{-3} kg and 4.328×10^{-3} kg at 7.5 and 12.5 V respectively, as shown in Table 5. The error between measured and predicted anode weight loss at 7.5 and 12.5 V is shown in Table 6 and also shows that z = 2 was much better in predicting the anode weight loss than z = 3, with error between 0.156–3.859% and 33.231–35.905% respectively. Therefore, the Fe^{2+} (ferrous) was generated through oxidation of iron during EC process and $z = 2$ was used in the mechanistic model. Similarly, Lakshmanan et al. [41] and Sasson et al. [42] arrived at the same conclusion that Fe^{2+} was generated at the iron anode during EC, not Fe^{3+}. The anode consumption at 12.5 V was 4.328×10^{-3} kg, which was more than the 2.241×10^{-3} kg at 7.5 V. This was due to the fact that higher voltage resulted in higher current density.

5.3. Temperature profile

Temperature of vinasse was measured per real time and profiled in Table 5. It increased till the end which was caused by the continuous supply of current during process. In addition, the effect of increasing the temperature at 12.5 V was faster than that at 7.5 V. Energy was supplied in solution could be estimated through Eq. (34).

$$Q = VIt \tag{34}$$

Therefore, the higher the I and t, the higher the Q would be. Based on Table 5, current value at 12.5 V was higher than that at 7.5 V. Relationship between Q and ΔT is presented in Eq. (35) [43,44].

$$\Delta T = \frac{Q}{C_p} \tag{35}$$

Hence, the higher the value of Q, the higher the increasing of temperature would be. Based on that, increasing rate of temperature at 12.5 V was higher than that at 7.5 V.

5.4. pH, COD, total dissolved Fe profile

Based on the discussion in Section 5.2, the appropriate value for z was 2, which resulted in the oxidation of iron into Fe^{2+} at the anode. Then, the Fe^{2+} reacted with OH^- ion to form insoluble coagulant of Fe $(OH)_2$ which adsorbed COD. Also, the Fe^{2+} could be oxidized to Fe^{3+} and then hydrolyzed to be $Fe(OH)_3$ [45,46]. However, according to Donneys-Victoria et al. [47], the formation of Fe^{3+} and $Fe(OH)_3$ occurs in pH range of 7.6-14. Besides that, the dissolved oxygen in solution could affect the oxidation of Fe^{2+} to Fe^{3+}, as shown in Eq. (36) [47].

$$4Fe^{2+} + O_2 + 2H_2O + 8OH^- \rightarrow 4Fe(OH)_3 \tag{36}$$

However, in this study, the pH range was 6.0–7.7, as shown in Table 5 and dissolved oxygen in the vinasse is very low [48]. Based on these conditions, the dominant iron species in system during EC process might be Fe^{2+} and $Fe(OH)_2$. Furthermore, the $Fe(OH)_2$ formed was assumed to be settled and floated sludge completely. Hence, total dissolved Fe measured through AAS was assumed as remaining total Fe^{2+} in solution.

During the EC, the reduction of H_2O resulted in the formation of OH^- ion and H_2 gas at cathode. However, the OH^- was not completely involved in the formation of $Fe(OH)_2$ and the excessive presence of OH^- increased the solution pH. In this case, the production of OH^- was higher than its consumption to produce coagulants. Based on the pH profile shown in Table 5, the pH increased from 6.0 to 7.2 from the beginning to the end of the EC process at 7.5 V. Meanwhile, at 12.5 V, the pH increased from 6.0 to 7.7 at 0 to 2400 s. Then, it was stable still at 7.7 from 2400 to 3000 s and finally decreased to 7.3 at 3600 s. This decrease in pH is caused by two ways: (1) the consumption rate of OH^- to produce hydroxo-iron species ($Fe(OH)_2$) is higher than its production rate [46,49] and (2) the OH^- is consumed by the hydroxo-iron species to produce anionic hydroxo-iron species ($Fe(OH)_3^-$ and $Fe(OH)_4^-$) [45,46,50,51]. The latter occurs at an alkaline pH because the Fe $(OH)_3^-$ and $Fe(OH)_4^-$ is formed at solution pH above 9.0 [21]. In this study, the solution pH, however, decreased from 7.7 to 7.3, which was in the neutral range, hence, the decrease in pH was only as a result of the former. This was consistent with the study of Soeprijanto et al. [49] in which the solution pH increased to7.43 and then decreased to 7.08.

The amount of Fe^{2+} formed was a function of the current supplied to the solution. Hence, voltage of 12.5 V produced larger amount of Fe^{2+}, thereby producing more $Fe(OH)_2$ and the COD mass removal was also higher than at voltage of 7.5 V, as shown in Table 5. Thus, the remaining total dissolved Fe in solution at 12.5 V was lower than at 7.5 V, as also shown in Table 5. This means that more Fe^{2+} became coagulant at 12.5 V than at 7.5 V. Then, in terms of pH, the increasing rate of solution pH at 12.5 V was higher than at 7.5 V and the higher the pH, the more Fe^{2+} became $Fe(OH)_2$. At neutral pH, gelatinous metal coagulant was released in large amount in solution [31,52].

5.5. Floated and settled sludge profile

The floated sludge generated during the EC process is shown in Table 5 and its appearance is shown in Fig. 6(A). The production of

Table 6
Measured and predicted electrode consumption after EC of vinasse waste at voltage of 7.5 and 12.5 V.

Voltage (V)	Measured data Anode weight loss ($\times 10^{-3}$ kg)	Predicted data			
		Anode weight loss ($\times 10^{-3}$ kg)		Error value on comparison with measured data (%)*	
		At z = 2	At z = 3	At z = 2	At z = 3
7.5	2.241	2.245	1.496	0.156	33.231
12.5	4.328	4.161	2.774	3.859	35.905

Note: * $Error\ (\%) = \frac{|Measured\ data - Predicted\ data|}{Measured\ data} 100\%$.

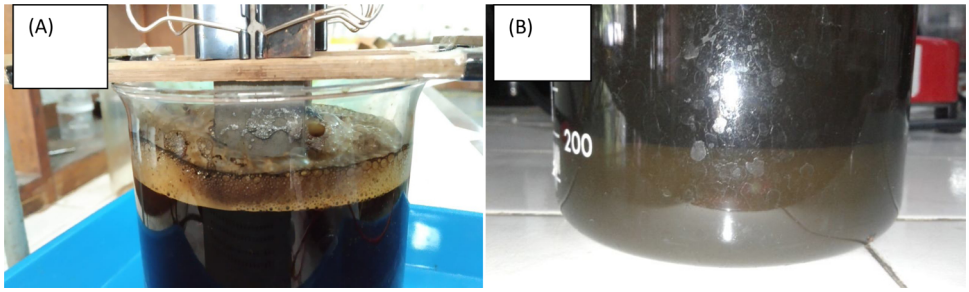

Fig. 6. Appearance of (A) floated sludge and (B) settled sludge production during EC of vinasse waste.

floated sludge at 12.5 V was higher than at 7.5 V. Based on the explanation in Section 5.4, H_2 gas was produced by reduction of water at cathode and the amount produced depended on the current supplied to the system. Based on Fig. 5(A), higher current density was supplied at 12.5 V than at 7.5 V. Therefore, more H_2 gas was produced at 12.5 V thereby allowing the pollutants to be easily separated by flotation at this higher voltage compared with 7.5 V. The amount of hydrogen production was predicted using Faraday's law as shown in Eq. (37), [53].

$$\frac{dn_{H_2}}{dt} = \frac{I}{F}H = \frac{JA_e}{F}H = \frac{J((2(l_e - bt)w_e + 2(l_e - bt)t_e + w_e t_e))}{F}H \quad (37)$$

The predicted production of H_2 during EC of vinasse is shown in Fig. 5(C). Based on this, more H_2 gas was produced at 12.5 V than at 7.5 V.

The settled sludge produced was predicted using Eq. (29a) and shown in Fig. 5(D). Then, its appearance is shown in Fig. 6(B), indicating more of settled sludge at 12.5 V than at 7.5 V. As explanation in Section 5.4, voltage of 12.5 resulted more coagulant of $Fe(OH)_2$ than voltage 7.5 V. The coagulant had correspondence to remove pollutants and then produced settled sludge.

5.6. Modeling

The proposed mechanistic models were successfully applied to fit the measured data. The fitting between the measured and predicted data obtained from the Model 1, Model 2, Model 3 and Model 4 is shown in Figs. 7–10 respectively. The adjustable parameters in Model 1 and Model 2 are k_a, k_e, k_f, the ones in Model 3 are k_a, k_e, k_s, while the ones in Model 4 are k_a, k_e, α. Furthermore, the kinetic parameters obtained from the four mechanistic models are presented in Table 7. Comparing the calculated results with the experimental data, it was obvious that all the proposed models were suitable for describing the phenomena, however, Model 2 mathematically and visually gave the best prediction. This was due to its lower SSE (0.1189-0.2289) compared with the others (0.1884-0.5792). These results showed that the mechanisms involved in pollutant removal in vinasse during EC process followed Model 2 as shown in Fig. 2.

The kinetic constant of b was obtained from Fig. 5(B), representing

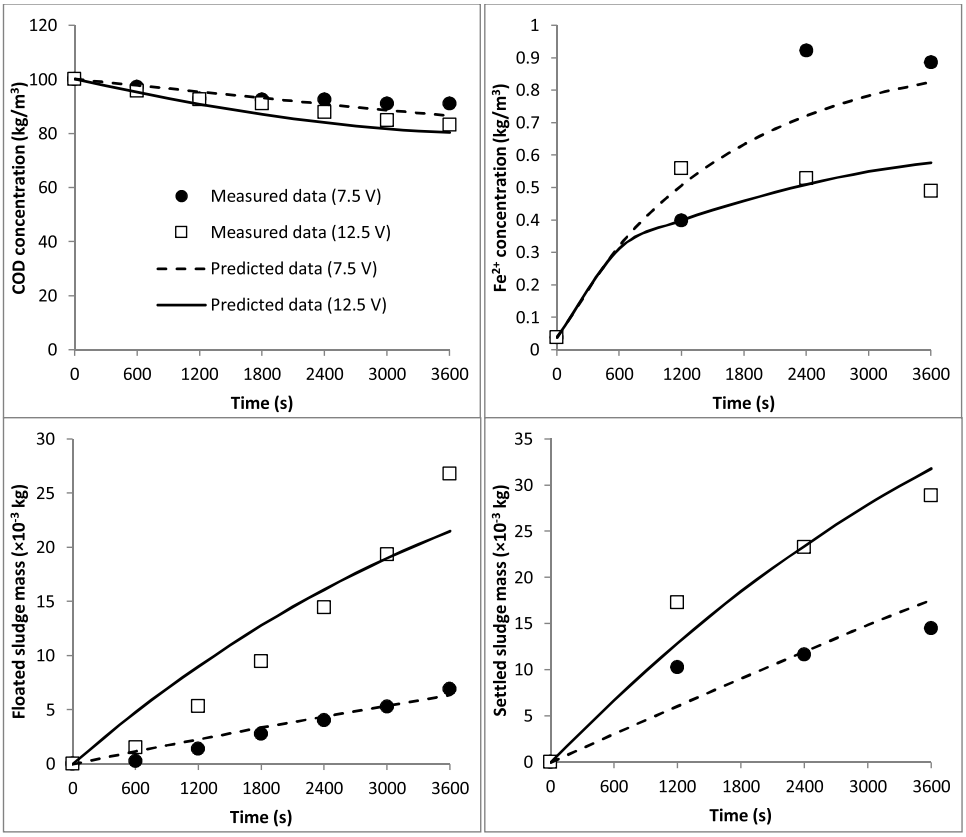

Fig. 7. Fitting between measured data and predicted data obtained from the Mechanistic Model 1 at voltage of 7.5 and 12.5 V during EC of vinasse waste.

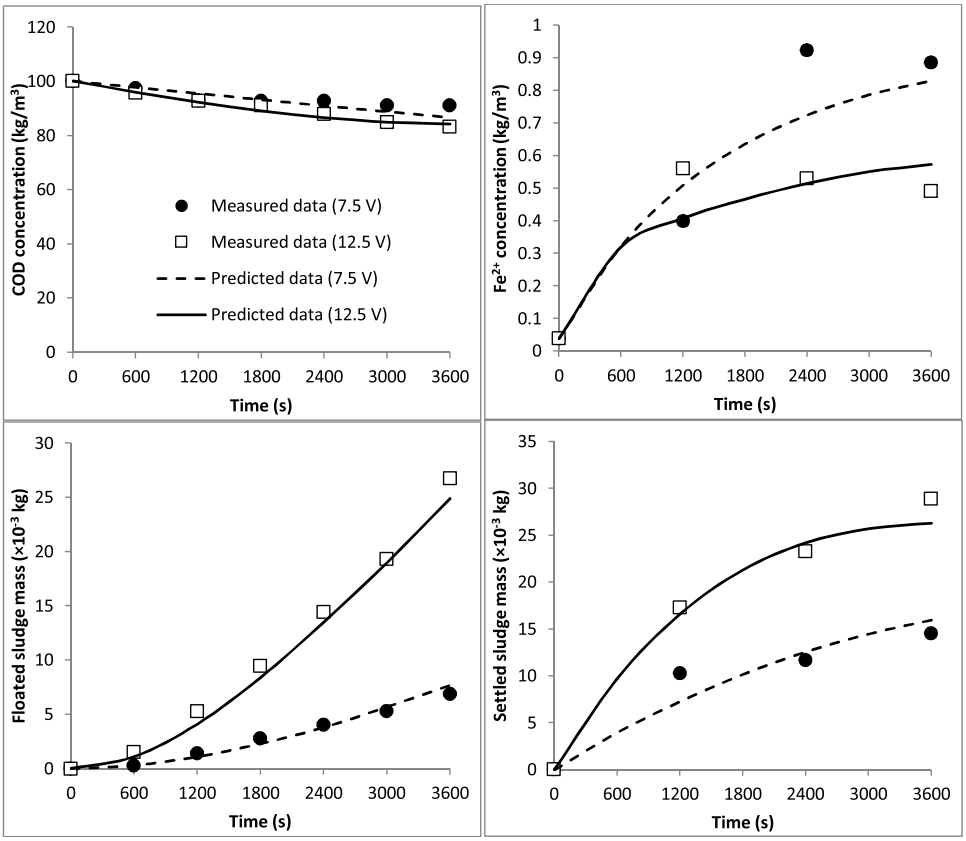

Fig. 8. Fitting between measured data and predicted data obtained from the Mechanistic Model 2 at voltage of 7.5 and 12.5 V during EC of vinasse waste.

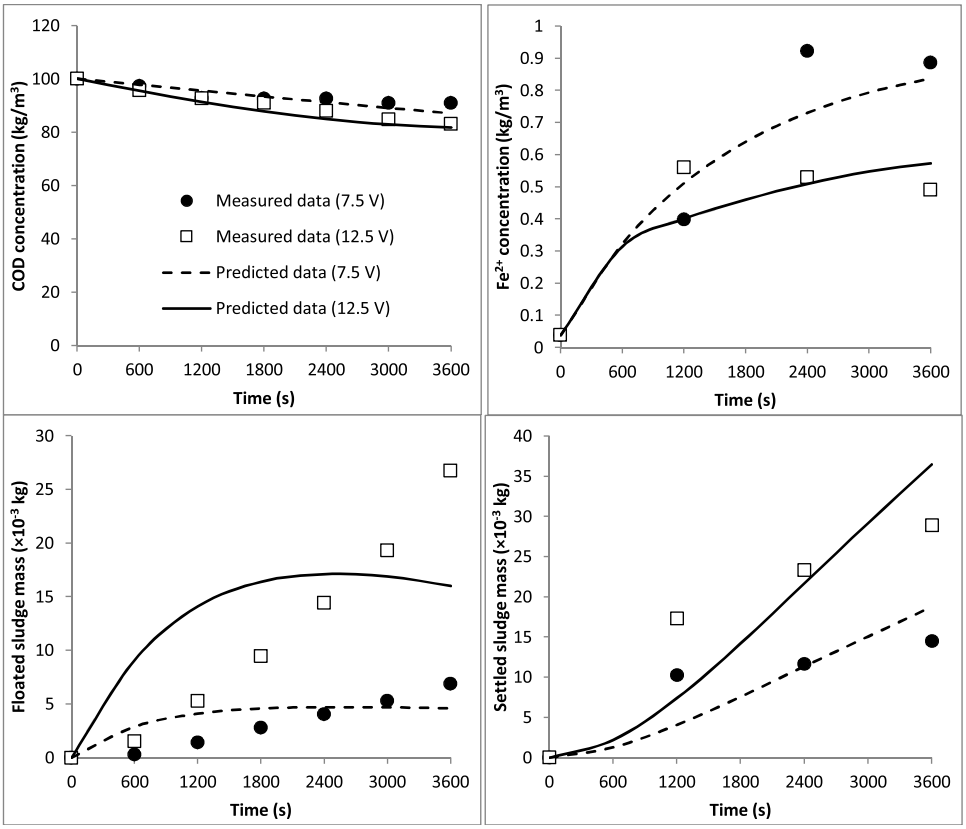

Fig. 9. Fitting between measured data and predicted data obtained from the Mechanistic Model 3 at voltage of 7.5 and 12.5 V during EC of vinasse waste.

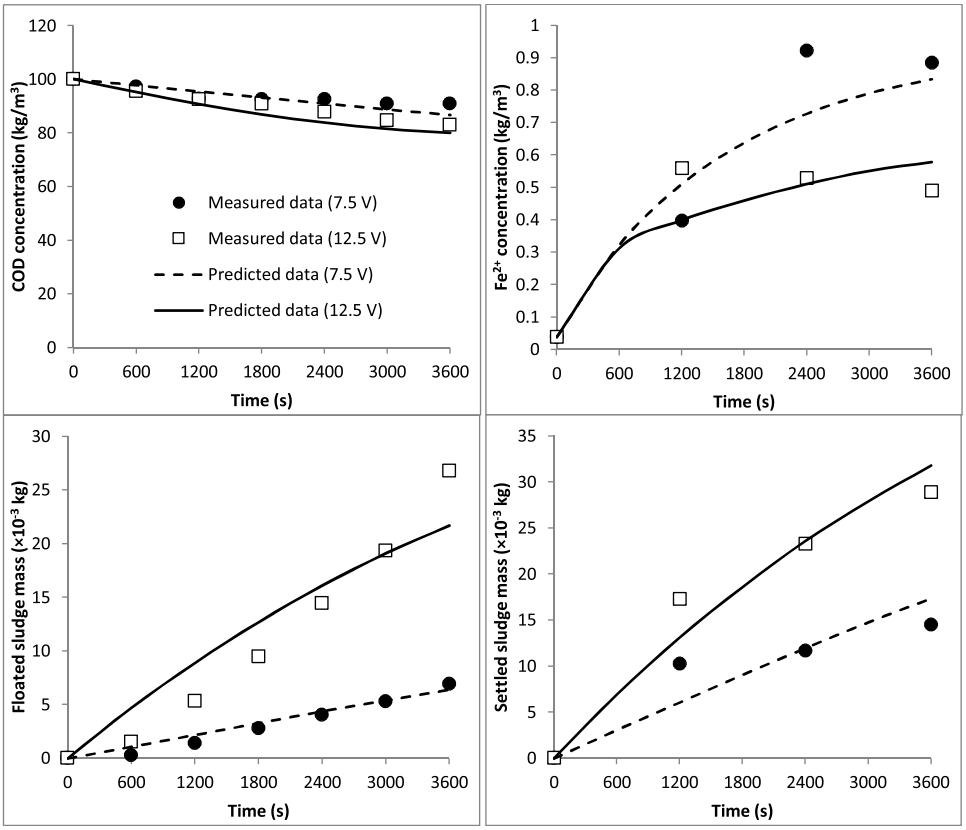

Fig. 10. Fitting between measured data and predicted data obtained from the Mechanistic Model 4 at voltage of 7.5 and 12.5 V during EC of vinasse waste.

Table 7
Kinetic parameter values for all mechanistic models at voltage 7.5 and 12.5 V in EC of vinasse waste.

Paramaters	Voltage	
	7.5 V	12.5 V
Model 1		
b (m/s)	0.351×10^{-5}	1.221×10^{-5}
k_a (m^3/(kg.s)	8.70×10^{-6}	3.78×10^{-5}
k_e (/s)	5.08×10^{-5}	1.11×10^{-4}
k_f (/s)	2.00×10^{-5}	8.59×10^{-5}
SSE	0.3361	0.1937
Model 2		
b (m/s)	0.351×10^{-5}	1.221×10^{-5}
k_a (m^3/(kg.s)	8.77×10^{-6}	3.64×10^{-5}
k_e (/s)	7.00×10^{-5}	1.84×10^{-4}
k_f (/s)	2.26×10^{-4}	3.70×10^{-4}
SSE	0.2289	0.1189
Model 3		
b (m/s)	0.351×10^{-5}	1.221×10^{-5}
k_a (m^3/(kg.s)	8.77×10^{-6}	3.73×10^{-5}
k_e (/s)	6.86×10^{-5}	1.90×10^{-4}
k_s (/s)	1.30×10^{-3}	7.36×10^{-4}
SSE	0.5792	0.5267
Model 4		
b (m/s)	0.351×10^{-5}	1.221×10^{-5}
k_a (m^3/(kg.s)	8.75×10^{-6}	3.77×10^{-5}
k_e (/s)	7.03×10^{-5}	1.96×10^{-4}
α (kg/kg)	0.7322	0.5941
SSE	0.3305	0.1884

the decreasing rate of vinasse surface level. In other words, the higher the b value, the more the volume was removed. Voltage of 12.5 V (1.221×10^{-5} m/s) resulted the more value of b than voltage of 7.5 V (0.351×10^{-5} m/s). This was due to the high current density as well as the high temperature at 12.5 V.

In Model 2, the k_a presented the reaction rate of adsorption of COD on coagulants. Its value at 12.5 V was 3.64×10^{-5} m^3/(kg.s) but was 8.77×10^{-6} m^3/(kg.s) at 7.5 V. As explanation in Section 5.4, amount of coagulants ($Fe(OH)_2$) produced at the higher voltage was more leading to faster adsorption rate of COD compared with the lower voltage.

In addition, the k_e in this model presented the entrapment rate of COD in forming settled sludge. It had a value of 1.84×10^{-4} /s at 12.5 V but was 7.00×10^{-5} /s at 7.5 V. The Fe^{2+} reacted with OH- to form coagulants which adsorbed the COD to form aggregates. These in turn dragged the other COD to settle at the base together as settled sludge. Hence, the more the aggregates in the system, the easier the COD was entrapped. More aggregates were formed at 12.5 V thereby resulting more settled sludge compared with 7.5 V.

Finally, the k_f in this model presented the flotation rate during EC process with a value of 3.70×10^{-4} /s at 12.5 V compared with 2.26×10^{-4} /s at 7.5 V. This was also caused by the higher current density at 12.5 V aiding the rapid formation of H_2, which broke the settled sludge and pushed it to the surface as floated sludge.

5.7. Comparison between the mechanistic model 2 and the empirical models

The first and second order kinetics, which are the two most popular empirical models, were also used to predict the COD concentration profile during EC. The predicted COD data from the empirical models and the Model 2 are shown in Table 8. The plotting between the measured COD and predicted COD by these models is shown in Fig. 11.

Based on the results, the first and second order kinetics gave good prediction with the almost same of Mean Absolute Percentage Error (MAPE) value which was 0.58–1.28 %. The Mechanistic Model 2, on the other hand, had a MAPE value of 0.82–1.85% (this value just obtained from COD concentration data). The formula for calculating MAPE is shown in Eq. (38). Despite the fact the COD profile predicted by the

Table 8
Results of predicted COD concentration by the Mechanistic Model 2, first order kinetic and second order kinetic in EC of vinasse waste.

Time (s)	7.5 V				12.5 V			
	Measured COD data (kg/m^3)	Predicted COD data (kg/m^3)			Measured COD data (kg/m^3)	Predicted COD data (kg/m^3)		
		Mechanistic Model 2	First order kinetic	Second order kinetic		Mechanistic Model 2	First order kinetic	Second order kinetic
0	100.16	100.16	100.16	100.16	100.16	100.16	100.16	100.16
600	97.36	97.89	98.27	98.14	95.79	96.03	96.95	96.89
1200	92.87	95.59	96.42	96.19	92.65	92.29	93.85	93.82
1800	92.65	93.31	94.61	94.32	91.08	89.13	90.85	90.95
2400	92.65	91.08	92.82	92.52	87.94	86.66	87.94	88.24
3000	91.08	88.90	91.08	90.79	84.80	84.97	85.12	85.69
3600	91.08	86.80	89.36	89.13	83.17	84.22	82.40	83.28
Kinetic constants								
k_1 (/s)	–	–	3.2×10^{-5}	–	–	–	5.4×10^{-5}	–
k_2(m^3/(kg.s))	–	–	–	3.4×10^{-7}	–	–	–	5.6×10^{-7}
MAPE (%)	–	1.85	1.28	1.25	–	0.82	0.58	0.59

Note: $MAPE = \frac{1}{n}\sum_{i=1}^{n}\left(\frac{|Measured\ COD_i - Predicted\ COD_i|}{Measured\ COD_i}\right)$ 100%.

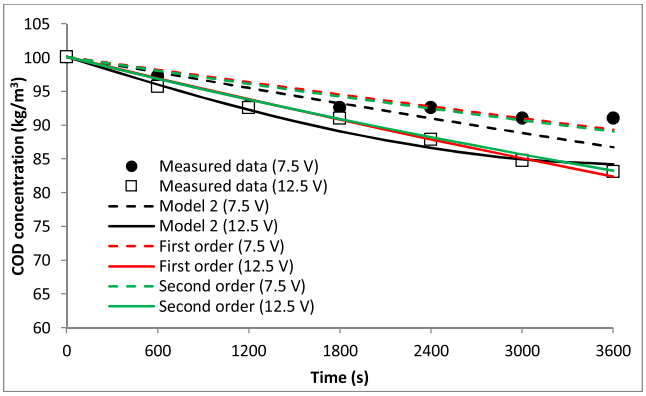

Fig. 11. Comparison among Mechanistic Model 2, first order kinetic and second order kinetic on fitting COD concentration profile during EC of vinasse waste.

empirical models was more precise compared with that of Mechanistic Model 2, the latter was very acceptable due to its low MAPE which was still below 2%. The maximum MAPE value in any modeling should not be more than 20% [54]. Furthermore, it could figure out detailed EC process with complete measured parameters including COD, total Fe, floated sludge and settled sludge profile during EC process, but the empirical models could not do that.

$$MAPE = \frac{1}{n}\sum_{i=1}^{n}\left(\frac{|Measured\ COD_i - Predicted\ COD_i|}{Measured\ COD_i}\right) 100\% \quad (38)$$

5.8. Estimation of the effect of charge loading on COD removal efficiency in EC of vinasse

The COD removal efficiency is mainly affected by the value of charge loading. Generally, the charge loading shows the charges transferred in electrochemical reactions for a given amount of wastewater treated. Commonly, it is calculated by Eq. (39) [55].

$$q = \frac{It}{v_{initial}} = \frac{JA_e t}{v_{initial}} \quad (39)$$

In this section, the results of many studies about EC of vinasse (also is known as distillery spent wash), including previous studies and this study, were summarized to see the effect of the charge loading on the COD removal efficiency. Because of the difference of initial COD concentration in their experiment, the Eq. (39) is modified to Eq. (40) by considering the initial COD concentration.

$$q = \frac{It}{v_{initial} C_{COD\ initial}} = \frac{JA_e t}{v_{initial} C_{COD\ initial}} \quad (40)$$

Table 9 shows the summary of experimental data from EC of vinasse from previous studies [56–62] and this study. For the purpose of simplifying the calculation, an average current of 2.15 and 3.99 A was used for variable of 7.5 V and 12.5 V respectively. The correlation between charge loading and COD removal efficiency is shown in Fig. 12. This showed that the increasing of charge loading from 0 to 18 × 10^5 C/kg COD required increase in the COD removal efficiency from 0 to 92.5%.

Table 9
Summary of experimental data in EC of vinasse waste from previous studies and this study with anode-cathode of Fe-Fe.

Initial COD (kg/m^3)	Initial pH	Initial volume (m^3)	Anode-Cathode	I (A)	A_e (m^2)	Voltage (V)	J (A/m^2)	agitation speed (rpm)	d (m)	t (s)	Charge loading (×10^5 C/kg COD)	COD removal efficiency (%)	References
52	7.2	0.0003	Fe-Fe	0.41	–	–	147	500	0.03	10800	2.84	76.9	[56]
128	3	0.001	Fe-Fe	–	0.00275	–	320	500	0.03	9000	0.62	73.17	[57]
2.5	7	0.002	Fe-Fe	–	0.01	–	13	100	0.03	14400	3.74	72	[58]
2.5	6	0.0005	Fe-Fe	–	0.0045	–	300	–	0.01	14400	155.52	62	[59]
2	6	0.002	Fe-Fe	–	0.01	–	10	–	0.02	14400	3.60	25.75	[60]
2	6	0.002	Fe-Fe	–	0.01	–	50	–	0.02	14400	18.00	92.5	[60]
3.36	7.5	0.0005	Fe-Fe	–	0.00128	3	718	500	0.03	7200	39.39	88	[61]
120	3	0.0003	Fe-Fe	–	0.0016	–	1875	500	0.03	7200	6.00	52.4	[62]
100.16	6	0.001	Fe-Fe	2.15*	–	7.5	–	200	0.055	3600	0.77	19.87	This study
100.16	6	0.001	Fe-Fe	3.99*	–	12.5	–	200	0.055	3600	1.43	51.67	This study

Note = *average value during process (this study).

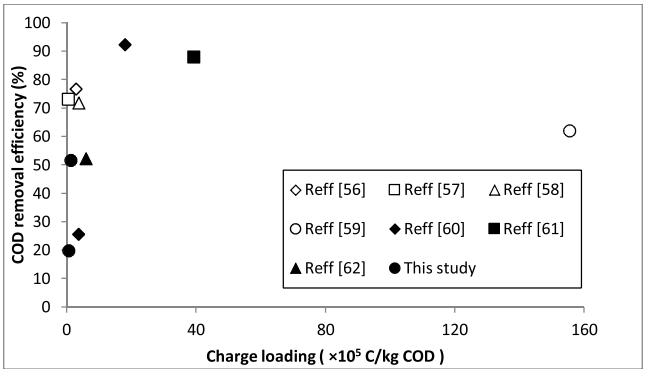

Fig. 12. Estimation of correlation between charge loading and COD removal efficiency in EC of vinasse.

However, further increase in the charge loading reduced the COD removal efficiency. It was noted that applying too high current was not good considering the fact it aided that excessive formation of hydrogen bubbles. The coagulants ($Fe(OH)_2$) formed could easily be pushed to the surface of solution by the hydrogen bubbles before they adsorbed and entrapped the pollutants. Too high current could also increase the solution temperature thereby causing the re-dissolution of the aggregates [63]. The COD concentration of vinasse in this study could be reduced from 100.16 to 83.17 kg/m^3, but still higher than the target concentration suitable as a biogas feedstock which is around 75 kg/m^3. Hence, there is need to conduct research on the other parameters affecting the EC process so as to achieve the target COD concentration.

6. Conclusion

This experiment research on EC of vinasse waste provided some information on the effect of voltage on current density, temperature, pH, COD, total dissolved Fe, floated and settled sludge during the process. In addition, the decrease in the working volume due to evaporation and reduction of water during EC was informed. The four mechanistic models were proposed to simulate the EC process with the assumption that some mechanisms such as electrode dissolution, adsorption, entrapment, sedimentation and flotation occurred in the system. These proposed mechanistic models were successfully applied to fit the measured data with different SSE values. However, Model 2 had the lowest SSE which means that COD removal mechanisms of this EC process for treating vinasse followed the Model 2. In addition, the kinetic constants in the model such as b (decreasing rate of vinasse height level), k_a (rate of adsorption), k_e (rate of entrapment) and k_f (rate of flotation) at 12.5 V was higher than that at 7.5 V. Furthermore, the Model 2 was compared with the first and second order kinetic models and the predicted COD from these three models was almost similar with very low MAPE value below 2%. However, the Model 2 was able to illustrate the COD removal mechanism in more details compared with the two empirical models. The correlation between the charge loading and COD removal efficiency in EC of vinasse was also successfully predicted. Moreover, there is need to conduct research on the other parameters affecting the COD removal from vinasse and then simulated using the Model 2 so as to find the kinetic constant values important in designing the EC systems for industrial use.

Declaration of Competing Interest

There are no competing interests to declare.

Acknowledgements

The authors thank to Lembaga Pengelola Dana Pendidikan (LPDP) Kementerian Keuangan Republik Indonesia via Beasiswa Unggulan Dosen Indonesia-Dalam Negeri (BUDI-DN) scholarship for financial support.

References

[1] V.G. de Barros, R.M. Duda, J. da Silva Vantini, W.P. Omori, M.I.T. Ferro, R.A. de Oliveira, Improved methane production from sugarcane vinasse with filter cake in thermophilic UASB reactors, with predominance of Methanothermobacter and Methanosarcina archaea and Thermotogae bacteria, Bioresour. Technol. 244 (2017) 371–381.
[2] J.A. Siles, I. García-García, A. Martín, M.A. Martín, Integrated ozonation and biomethanization treatments of vinasse derived from ethanol manufacturing, J. Hazard. Mater. 188 (2011) 247–253.
[3] K. Lutoslawki, A. Ryznar-Luty, E. Cibis, M. Krzywonos, T. Miskiewicz, Biodegradation of beet molasses vinasse by a mixed culture of microorganisms: effect of aeration conditions and pH control, J. Environ. Sci. 23 (11) (2011) 1823–1830.
[4] I. Syaichurrozi, Budiyono, S. Sumardiono, Predicting kinetic model of biogas production and biodegradability organic materials: biogas production from vinasse at variation of COD/N ratio, Bioresour. Technol. 149 (2013) 390–397.
[5] I. Syaichurrozi, Review – biogas technology to treat bioethanol vinasse, Waste Technol. 4 (1) (2016) 16–23.
[6] Budiyono, I. Syaichurrozi, S. Sumardiono, Effect of total solid content to biogas production rate from vinasse, Int. J. Eng. 27 (2) (2014) 177–184.
[7] I. Syaichurrozi, Budiyono, S. Sumardiono, Predicting kinetic model of biogas production and biodegradability organic materials: biogas production from vinasse at variation of COD/N ratio, Bioresour. Technol. 149 (2013) 390–397.
[8] V. Robles-González, J. Galíndez-Mayer, N. Rinderknecht-Seijas, H.M. Poggi-Varaldo, Treatment of mezcal vinasses: a review, J. Biotechnol. 157 (2012) 524–546.
[9] K.C. dos Reis, J.M. Coimbra, W.F. Duarte, R.F. Schwan, C.F. Silva, Biological treatment of vinasse with yeast and simultaneous production of single-cell protein for feed supplementation, Int. J. Environ. Sci. Technol. 16 (2019) 763–774.
[10] D.C. Hakika, S. Sarto, A. Mindaryani, M. Hidayat, Decreasing COD in sugarcane vinasse using the Fenton reaction: the effect of processing parameters, Catalysts 9 (2019) 881.
[11] C.E.R. Reis, H.B.S. Bento, T.M. Alves, A.K.F. Carvalho, H.F. De Castro, Vinasse treatment within the sugarcane-ethanol industry using ozone combined with anaerobic and aerobic microbial processes, Environments 6 (2019) 5.
[12] I. Syaichurrozi, S. Sarto, W.B. Sediawan, M. Hidayat, Mechanistic model of electrocoagulation process for treating vinasse waste: Effect of initial pH, J. Environ. Chem. Eng. 8 (2020) 103756.
[13] E. Demirbas, M. Kobya, Operating cost and treatment of metalworking fluid wastewater by chemical coagulation and electrocoagulation processes, Process. Saf. Environ. Prot. 105 (2017) 79–90.
[14] M. Elazzouzi, Kh. Haboubi, M.S. Elyoubi, Electrocoagulation flocculation as a low-cost process for pollutants removal from urban wastewater, Chem. Eng. Res. Des. 117 (2017) 614–626.
[15] B.-Y. Tak, B.-S. Tak, Y.-J. Kim, Y.-J. Park, Y.-H. Yoon, G.-H. Min, Optimization of color and COD removal from livestock wastewater by electrocoagulation process: application of Box–Behnken design (BBD), J. Ind. Eng. Chem. 28 (2015) 307–315.
[16] K.S. Hashim, R. AlKhaddar, A. Shaw, P. Kot, D. Al-Jumeily, R. Alwash, M.H. Aljefery, Electrocoagulation as an eco-friendly river water treatment method, Advances in Water Resources Engineering and Management, Springer, Singapore, 2020, pp. 219–235.
[17] K.S. Hashim, A.H. Hussein, S.L. Zubaidi, P. Kot, L. Kraidi, R. Alkhaddar, A. Shaw, R. Alwash, Effect of initial pH value on the removal of reactive black dye from water by electrocoagulation (EC) method, J. Phys. Conf. Ser. 1294 (September) (2019) 072017.
[18] B.A. Abdulhadi, P. Kot, K.S. Hashim, A. Shaw, R. Al Khaddar, Influence of current density and electrodes spacing on reactive red 120 dye removal from dyed water using electrocoagulation/electroflotation (EC/EF) process, IOP Conference Series: Materials Science and Engineering 584 (2019) 012035.
[19] K.S. Hashim, N.H. Al-Saati, S.S. Alquzweeni, S.L. Zubaidi, P. Kot, L. Kraidi, A.H. Hussein, R. Alkhaddar, A. Shaw, R. Alwash, Decolourization of dye solutions by electrocoagulation: an investigation of the effect of operational parameters, IOP Conference Series: Materials Science and Engineering 584 (2019) 012024.
[20] K.S. Hashim, A. Shaw, R. Al Khaddar, M.O. Pedrola, D. Phipps, Defluoridation of drinking water using a new flow column-electrocoagulation reactor (FCER)-Experimental, statistical, and economic approach, J. Environ. Manage. 197 (2017) 80–88.
[21] S. Garcia-Segura, M.M.S.G. Eiband, J.V. de Melo, C.A. Martínez-Huitle, Electrocoagulation and advanced electrocoagulation processes: a general review about the fundamentals, emerging applications and its association with other technologies, J. Electroanal. Chem. 801 (2017) 267–299.
[22] L. Largitte, R. Pasquier, A review of the kinetics adsorption models and their

application to the adsorption of lead by an activated carbon, Chem. Eng. Res. Des. 109 (2016) 495–504.
[23] Y.A. Ouaissa, M. Chabani, A. Amrane, A. Bensmaili, Removal of tetracycline by electrocoagulation: kinetic and isotherm modeling through adsorption, J. Environ. Chem. Eng. 2 (2014) 177–184.
[24] M.A. Mamelkina, F. Vasilyev, R. Tuunila, M. Sillänpää, A. Häkkinen, Investigation of the parameters affecting the treatment of mining waters by electrocoagulation, J. Water Process. Eng. 32 (2019) 100929.
[25] E.L. Fernández, E.M. Merlo, L.R. Mayor, J.V. Camacho, Kinetic modelling of a diesel-polluted clayey soil bioremediation process, Sci. Total Environ. 557–558 (2016) 276–284.
[26] J.N. Hakizimana, B. Gourich, M. Chafi, Y. Stiriba, C. Vial, P. Drogui, J. Naja, Electrocoagulation process in water treatment: a review of electrocoagulation modeling approaches, Desalination 404 (2017) 1–21.
[27] M. Dolati, A.A. Aghapour, H. Khorsandi, S. Karimzade, Boron removal from aqueous solutions by electrocoagulation at low concentrations, J. Environ. Chem. Eng. 5 (5) (2017) 5150–5156.
[28] H. Singh, B.K. Mishra, Assessment of kinetics behavior of electrocoagulation process for the removal of suspended solids and metals from synthetic water, Environ. Eng. Res. 22 (2) (2017) 141–148.
[29] M. Al-Shannag, Z. Al-Qodah, K. Bani-Melhem, M.R. Qtaishat, M. Alkasrawi, Heavy metal ions removal from metal plating wastewater using electrocoagulation: kinetic study and process performance, Chem. Eng. J. 260 (2015) 749–756.
[30] N.S.M. Amdan, N.S.M. Zin, S.N.A.M. Salleh, L.W.M. Zailani, Addition of composite coagulant (polyaluminium chloride and tapioca flour) into electrocoagulation (aluminium and ferum electrodes) for treatment of stabilized leachate, MATEC Web of Conferences 250 (2018), p. 06005.
[31] C. David, M. Arivazhagan, F. Tuvakara, Decolorization of distillery spent wash effluent by electrooxidation (EC and EF) and Fenton processes: a comparative study, Ecotoxicol. Environ. Saf. 121 (2015) 142–148.
[32] Office of Saline Water, Research and Development Progress Report, U.S. Department of the Interior, University of Michigan, 1969, https://books.google.co.id/books?id=rJXVAAAAMAAJ&source=gbs_navlinks_s.
[33] M.P. Wagh, P.D. Nemade, S.R. Dhasal, Colour and COD removal of distillery spent wash by using electro coagulation, Int. J. Eng. Res. Gen. Sci. 3 (3) (2015) 1159–1173.
[34] Radiometer Analytical SAS, Conductivity Theory and Practice, (2004) https://www.tau.ac.il/~chemlaba/Files/Theoryconductivity.pdf (Online 18 October 2019).
[35] R. Parga, D.L. Cocke, V. Valverde, Characterization of electrocoagulation for removal of chromium and arsenic, Chem. Eng. Technol. 28 (5) (2005) 605–612.
[36] M.Y. Mollah, R. Schennach, J.R. Parga, D.L. Cocke, Electrocoagulation science and applications, J. Hazard. Mater. 84 (1) (2001) 29–41.
[37] M.A. Mamelkina, R. Tuunila, M. Sillänpää, A. Häkkinen, Systematic study on sulfate removal from mining waters by electrocoagulation, Sep. Purif. Technol. 216 (2019) 43–50.
[38] C. Pan, L.D. Troyer, J.G. Catalano, D.E. Giammar, Dynamics of Chromium (VI) removal from drinking water by iron electrocoagulation, Environ. Sci. Technol. 50 (24) (2016) 13502–13510.
[39] M. Kobya, E. Senturk, M. Bayramoglu, Treatment of poultry slaughterhouse wastewaters by electrocoagulation, J. Hazard. Mater. 133 (1) (2006) 172–176.
[40] M.Y. Mollah, P.G. Morkovsky, A.G. Gomes, M. Kesmez, J. Parga, Fundamentals, present and future perspectives of electrocoagulation, J. Hazard. Mater. 114 (1-3) (2004) 199–210.
[41] D. Lakshmanan, D.A. Clifford, G. Samanta, Ferrous and ferric ion generation during iron electrocoagulation, Environ. Sci. Technol. 43 (2009) 3853–3859.
[42] M.B. Sasson, W. Calmano, A. Adina, Iron-oxidation processes in an electroflocculation (electrocoagulation) cell, J. Hazard. Mater. 171 (2009) 704–709.
[43] O. Larue, E. Vorobiev, Floc size estimation in iron induced electrocoagulation and coagulation using sedimentation data, Int. J. Mineral Proc. 71 (2003) 1–15.
[44] M.F. Ni'am, F. Othman, J. Sohaili, Z. Fauzia, Electrocoagulation technique in enhancing COD and suspended solids removal to improve wastewater quality, Water Sci. Technol. 56 (7) (2007) 47–53.
[45] D. Ghernaout, A.I. Al-Ghonamy, M. Wahib, Naceur, N.A. Messaoudene, M. Aichouni, Influence of operating parameters on electrocoagulation of C.I. disperse yellow 3, J. Electrochem. Sci. Eng. 4 (4) (2014) 271–283.
[46] I. Kabdaşlı, I. Arslan-Alaton, T. Ölmez-Hancı, O. Tünay, Electrocoagulation applications for industrial wastewaters: a critical review, Environ. Technol. Rev. 1 (1) (2012) 2–45.
[47] D. Donneys-Victoria, N. Marriaga-Cabrales, F. Machuca-Martinez, Electrocoagulation for landfill leachate treatment: a review of patents and research articles, Res. Signpost (2014) 17–39.
[48] J.F. Pires, G.M.R. Ferreira, K.C. Reis, R.F. Schwan, C.F. Silva, Mixed yeasts inocula for simultaneous production of SCP and treatment of vinasse to reduce soil and fresh water pollution, J. Environ. Manage. 182 (2016) 455–463.
[49] Soeprijanto, A.D. Perdani, D.F. Nury, L. Pudjiastuti, Treatment of oily bilge water by electrocoagulation process using aluminum electrodes, AIP Conference Proceedings 1840 (2017) 110015.
[50] K. Mansouri, A. Hannachi, A. Abdel-Wahab, N. Bensalah, Electrochemically dissolved aluminum coagulants for the removal of natural organic matter from synthetic and real industrial wastewaters, Ind. Eng. Chem. Res. 51 (2012) 2428–2437.
[51] K. Brahmi, W. Bouguerra, B. Hamrouni, E. Elaloui, M. Loungou, Z. Tlili, Investigation of electrocoagulation reactor design parameters effect on the removal of cadmium from synthetic and phosphate industrial wastewater, Arab. J. Chem. 12 (2019) 1848–1859.
[52] E. Nariyan, A. Aghababaei, M. Sillanpää, Removal of pharmaceutical from water with an electrocoagulation process; effect of various parameters and studies of isotherm and kinetic, Sep. Purif. Technol. 188 (2017) 266–281.
[53] C. Phalakornkule, P. Sukkasem, C. Mutchimsattha, Hydrogen recovery from the electrocoagulation treatment of dye-containing wastewater, Int. J. Hydrogen Energy 35 (2010) 10934–10943.
[54] I. Syaichurrozi, S. Suhirman, T. Hidayat, Effect of initial pH on anaerobic co-digestion of Salvinia molesta and rice straw for biogas production and kinetics, Biocatal. Agric. Biotechnol. 16 (2018) 594–603.
[55] M. Kobya, E. Demirbas, F. Ulu, Evaluation of operating parameters with respect to charge loading on the removal efficiency of arsenic from potable water by electrocoagulation, J. Environ. Chem. Eng. 4 (2) (2016) 1484–1494.
[56] V. Khandegar, A.K. Saroh, Treatment of distillery spentwash by electrocoagulation, J. Clean Energy Technol. 2 (3) (2014) 244–247.
[57] M.P. Wagh, P.D. Nemade, Treatment of distillery spent wash by using chemical coagulation (CC) and electro - coagulation [EC], Am. J. Environ. Prot. 3 (5) (2015) 159–163.
[58] P. Asaithambi, B. Sajjadi, A.R.A. Aziz, W.M.A.B.W. Daud, Performance evaluation of hybrid electrocoagulation process parameters for the treatment of distillery industrial effluent, Process. Saf. Environ. Prot. 104 (Part A) (2016) 406–412.
[59] P. Asaithambi, M. Susree, R. Saravanathamizhan, M. Matheswaran, Ozone assisted electrocoagulation for the treatment of distillery effluent, Desalination 297 (2012) 1–7.
[60] A.R.A. Aziz, P. Asaithambi, W.M.A.B.W. Daud, Combination of electrocoagulation with advanced oxidation processes for the treatment of distillery industrial effluent, Process. Saf. Environ. Prot. 99 (2016) 227–235.
[61] V. Khandegar, A.K. Saroha, Electrocoagulation of distillery spentwash for complete organic reduction, Int. J. Chemtech Res. 5 (2) (2013) 712–718.
[62] V. Khandegar, A.K. Saroha, Electrochemical treatment of distillery spent wash using aluminum and iron electrodes, Chin. J. Chem. Eng. 20 (3) (2012) 439–443.
[63] M.K. Purkait, P. Mondal, C.-T. Chang, Treatment of Industrial Effluents: Case Studies, CRC Press, 2009.